Available online at www.sciencedirect.com
SCIENCE DIRECT
Polymer 46 (2005) 11820–11828
polymer
www.elsevier.com/locate/polymer

Effects of polyoxyethylene nonylphenol on dynamic mechanical properties and crystallization of polypropylene

Qing-Xin Zhang [a,*], Jian-Bin Song [b], Shu-Yun Wang [b], Zhi-Shen Mo [b]

[a] School of Aerospace, Mechanical and Mechatronic Engineering, J07, The University of Sydney, Sydney, NSW 2006, Australia
[b] State Key Laboratory of Polymer Physics and Chemistry, Changchun Institute of Applied Chemistry, Chinese Academy of Sciences, Changchun, China

Received 14 May 2005; received in revised form 12 September 2005; accepted 10 October 2005
Available online 26 October 2005

Abstract

Polypropylene (PP) was blended with polyoxyethylene nonylphenol (PN) in a twin-screw extruder and injection moulded. The dynamic mechanical properties of PP/PN blends were characterized by dynamic mechanical analyser (DMA). The glass transition temperature (T_g) of PP showed a slight decrease with incorporation of PN. Differential scanning calorimetry (DSC), wide angle X-ray diffraction (WAXD) and polarized optical microscopy (POM) were employed to investigate the effects of PN on crystallization of PP. In a study of nonisothermal crystallization of PP and PP/PN blends, crystallization parameter analysis showed the addition of PN reduced the peak temperature of crystallization. β-form crystals of PP coexisted with α-form crystals in PP/PN blends, and oriented on the surface layer of injection moulded bar as revealed by WAXD. The degree of orientation was determined using Hermans orientation function. The thermal stability of β-form crystals was evaluated using high temperature WAXD and POM.

Keywords: Polypropylene; Polyoxyethylene nonylphenol; Crystallization

1. Introduction

PP is a widely used, versatile, commodity polymer with a number of desirable properties, i.e. high chemical resistance, fine mechanical properties, low cost, good environment stability in addition to its fine processability. PP is known to exhibit several crystalline forms, namely the monoclinic α-form, the hexagonal β-form and the triclinic γ-form [1]. In all of these structures, the chain conformation of each individual molecular chain is believed to be identical with a 3_1 helical conformation [1,2]. The different crystal structures are distinct due to the different chain packing geometries of the helices. It has been proved that the crystallization behaviour of the semi-crystalline phase in PP has a significant influence on mechanical properties i.e. the β-form PP exhibits much higher impact toughness than the α-form PP [1,3].

In melt crystallized PP, the predominant crystal structure is the monoclinic α-form. The crystal unit cell of the α-form are $a=0.6666$ nm, $b=2.078$ nm, $c=0.6495$ nm, $\beta=99.6°$ with a crystallographic symmetry of $P2_1/c$, reported by Turner-Jones et al. [4], which represents a small change from those originally reported by Natta and Corradini [5]. The hexagonal β-form occurs much more rarely than the α-form. In most cases, the β-form can only be partially formed in samples mixed with α-form. The β-form can be obtained by rapid quenching [6] or introducing β-form nucleating agents such as calcium carbonate [7,8], or blends of pimelic acid and calcium stearate [3,9,10]. The β-form generally shows two diffractions at *d*-spacings of 0.553 and 0.417 nm, and these two peaks are believed to fit into a hexagonal lattice with $a=1.274$ nm and $c=0.635$ nm [11]. It is also suggested that the hexagonal lattice should possess a unit cell of $a=2.203$ nm and $c=0.649$ nm [12]. The reported crystal unit cells of β-form are controversial. One important reason is that the β-form crystal is thermodynamically less stable than the α-form under normal crystallization conditions. The γ-form usually appears under high pressure [13,14]. The triclinic cell geometry of the γ-form, which has been widely accepted with the unit cell as proposed by Morrow and Newman [15], has the cell dimensions of $a=0.654$ nm, $b=2.140$ nm, $c=0.650$ nm, $\alpha=89°$, $\beta=99.6°$ and $\gamma=99°$.

Polyoxyethylene nonylphenol is one important member of the nonionic surfactants family which possesses a hydrophobic

* Corresponding author. Fax: +61 2 9351 7060.
E-mail address: drzhqx@yahoo.com (Q.-X. Zhang).

0032-3861/$ - see front matter © 2005 Elsevier Ltd. All rights reserved.
doi:10.1016/j.polymer.2005.10.057

hydrocarbon end and a hydrophilic hydroxyl end. Polyoxyethylene nonylphenols have been widely used in plastic and textile industry as antistatic agent, dispersing agent or emulsifying agent because of its special chemical structure [16–21]. However, there are few articles in the literature known to us, which address the effects of polyoxyethylene nonylphenol on dynamic mechanical properties and crystallization behaviour of PP. In our previous study, we found that the nonionic surfactant polyoxyethylene nonylphenol is very helpful to improve nano $CaCO_3$ particle dispersion in PP [21]. In this work, the effects of polyoxyethylene nonylphenol on dynamic mechanical properties and crystallization of PP were investigated.

2. Experimental

2.1. Sample preparation

PP was provided by ICI Australia Operations. The original pellets have a tradename of GWM 22 and a density of 0.96 g/cm^3. The nonionic surfactant, polyoxyethylene nonylphenol with density of 1.02 g/cm^3, was obtained as light yellow liquid from Tianjin Feejy Trade Co., Ltd, China with the following structural formula:

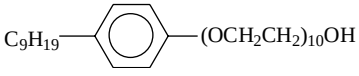

PP pellets and polyoxyethylene nonylphenol were melt compounded in desired compositions in a co-rotating Werner and Pfleider ZSK-30 twin screw extruder at temperatures in a range of 190–200 °C and a screw rotation rate of 300 rpm. The material compositions were shown in Table 1. The extrudates were pelletized at the die exit, dried and then injection moulded into standard dumbbell tensile bars (50 mm gauge length, 10 mm width, and 3 mm thickness) by a BOY 22s dipronic injection moulding machine whose barrel temperature was kept at 200 °C and the mould 60 °C.

2.2. DMA

Measurements of DMA were made using a single cantilever beam fixture under cyclic loading at 1 Hz on a TA Instruments DMA 2980 system. All the runs were conducted at 3 °C/min from -40 to 50 °C under N_2 atmosphere.

2.3. DSC

Samples of about 10 mg were sealed in aluminum pans. DSC measurements were carried out on a TA 2920 DSC with a sealed empty pan as the reference and under a nitrogen atmosphere. Nonisothermal crystallization was performed as follows: the samples of about 10 mg were heated to 200 °C and maintained at this temperature for 5 min to eliminate any previous thermal history, and then cooled to 50 °C at a cooling rate of 10 °C/min.

Table 1
Compositions of PP/PN blends

Designation in this work	PN content (wt%)
PP	0
PP-0.75	0.75
PP-1.50	1.50
PP-2.25	2.25

2.4. POM

The PP/PN blend (0.75 wt%) was sandwiched in between microscopic slides and quenched in air to room temperature (RT) after melt at 200 °C for 5 min. Then the morphology of PP spherulites was recorded in a LEITZ DMRXE polarized optical microscopy (POM) equipped with a hot stage with a heating rate of 10 °C/min from room temperature to 200 °C.

2.5. WAXD

The WAXD specimens were cut from dumbbell tensile bars. WAXD experiments at room temperature were performed using a Siemens D5000 diffractometer operated at 40 kV and 30 mA ($\lambda = 0.15406$ nm). High temperature WAXD from 20–180 °C were obtained by a Rigaku D/max 2500V X-ray diffractometer in combination with an 18 kW

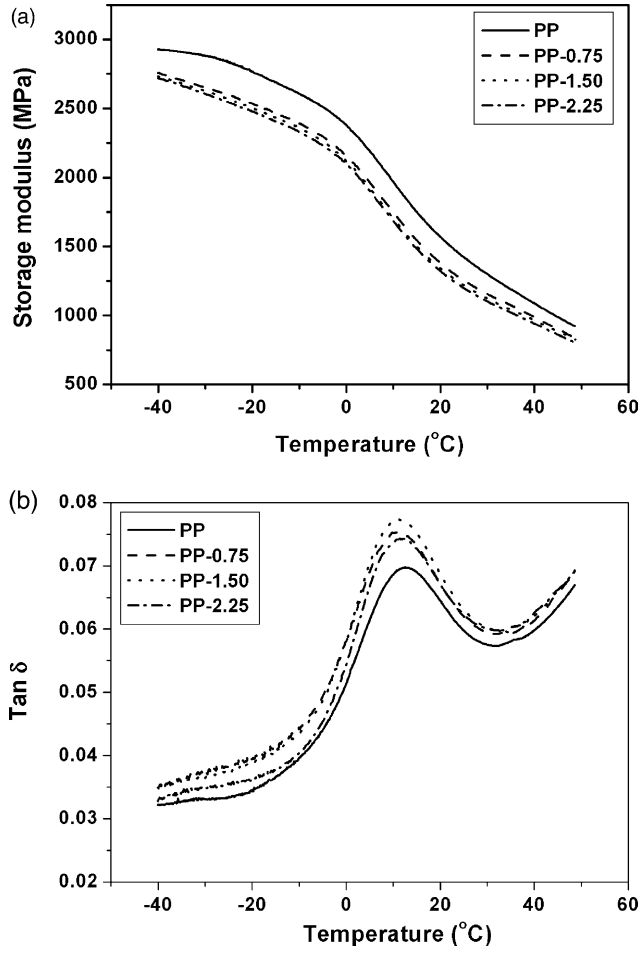

Fig. 1. Storage modulus as a function of temperature for PP and PP/PN blends (a) and tan δ as a function of temperature for PP and PP/PN blends (b).

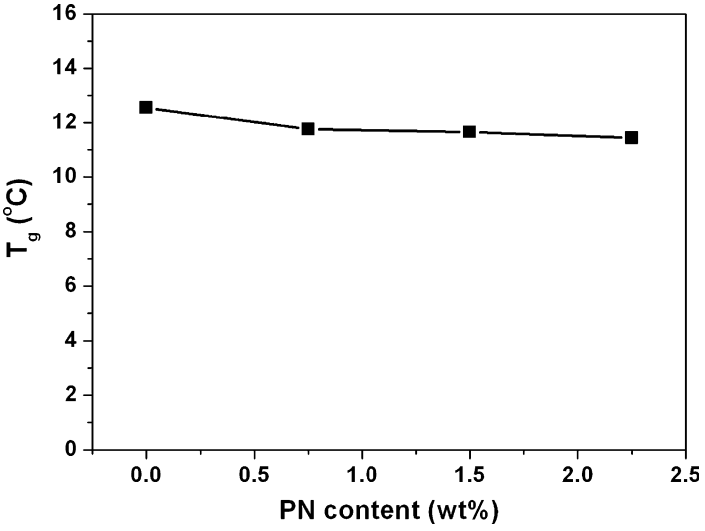

Fig. 2. Glass transition temperatures (T_g) of PP and PP/PN blends.

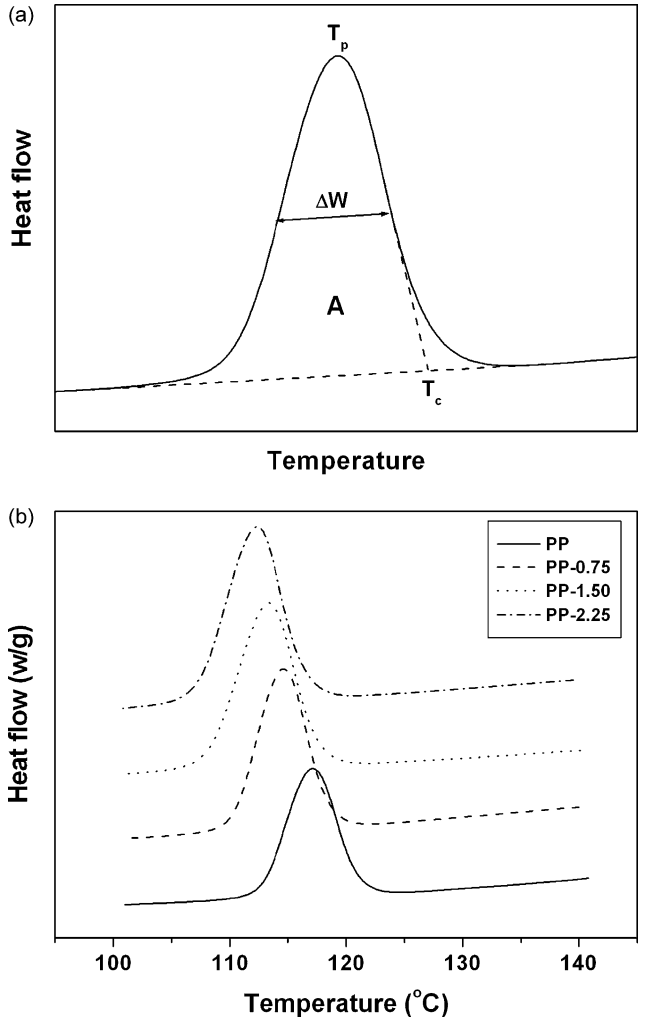

Fig. 3. Schematic representation of nonisothermal crystallization parameters from DSC crystallization exotherm peak (a), and normalized nonisothermal crystallization thermograms of PP and PP/PN blends (cooling rate = 10 °C/min) (b).

Table 2
Nonisothermal crystallization parameters of PP and PP/PN blends at cooling rate of 10 °C/min

Sample	T_p (°C)	T_c (°C)	$T_c - T_p$ (°C)	A	ΔW
PP	117.08	121.96	4.88	4.92	4.05
PP-0.75	114.55	119.25	4.70	6.08	4.01
PP-1.50	113.16	117.80	4.64	7.06	4.59
PP-2.25	112.14	116.50	4.36	7.23	4.46

rotating-anode generator and curved graphite crystal filtered Cu Kα_1 radiation ($\lambda = 0.15406$ nm). The heating rate was 10 °C/min and the cooling rate was 5 °C/min. All the WAXD data were collected from $2\theta = 10$–30° with a step interval of 0.02°.

A thin section with thickness of 0.3 mm was obtained from a PP/PN tensile bar surface parallel to the injection moulding direction and the flat surface to evaluate the crystals orientation. Imaging plate (IP), with size of 127 × 127 mm, was supplied by Fuji Photo Films Co. Ltd. IP measurement was performed with the diffractometer operating at 50 kV and 100 mA. In the X-ray diffraction system, intensity data were read out as digital values so that they are readily processed with a computer. Subsequently, the WAXD pattern was analyzed by Rigaku R-AXIS Display Software.

3. Results and discussion

3.1. Dynamic mechanical properties

DMA was employed to measure the dynamic response of the PP/PN blends under a given set of conditions. The analysis of the storage modulus and loss tangent (tan δ) curves is very useful in ascertaining the performance of the sample under stress and temperature. Storage modulus is directly associated with elastic response and tan δ is related with the molecular chain relaxation that takes place. Fig. 1 (a) and (b) present the

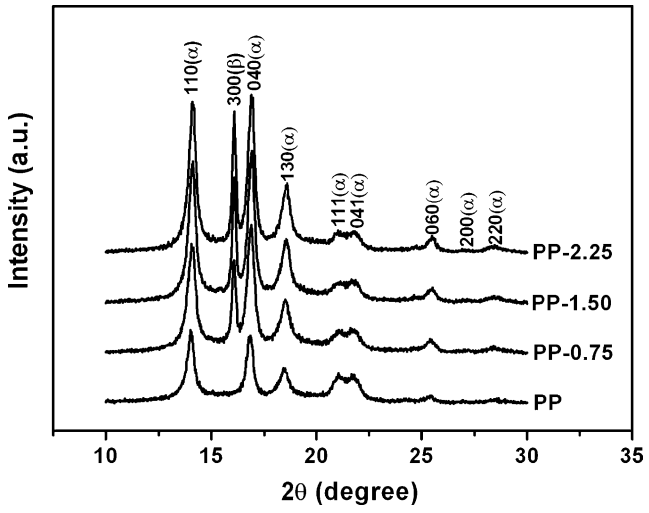

Fig. 4. WAXD curves of neat PP as well as PP/PN blends.

Table 3
WAXD parameters for PP and PP/PN blends

Sample	Diffraction peak	2θ (°)	d (Å)	β_{hkl}	L_{hkl} (Å)	K (%)
PP	110(α)	13.98	6.33	0.26	5.32	0
	040(α)	16.80	5.24	0.29	4.72	
	130(α)	18.46	4.80	0.41	3.36	
PP-0.75	110(α)	14.06	6.29	0.35	3.96	14.1
	300(β)	16.08	5.51	0.12	11.87	
	040(α)	16.90	5.24	0.31	4.54	
	130(α)	18.50	4.79	0.40	3.45	
PP-1.50	110(α)	14.10	6.28	0.31	4.53	15.7
	300(β)	16.08	5.51	0.10	13.92	
	040(α)	16.92	5.24	0.29	4.72	
	130(α)	18.54	4.78	0.43	3.19	
PP-2.25	110(α)	14.08	6.28	0.28	4.89	16.2
	300(β)	16.08	5.51	0.10	13.92	
	040(α)	16.90	5.24	0.29	4.72	
	130(α)	18.60	4.77	0.42	3.27	

storage modulus and the tan δ of PP and PP/PN blends respectively. The PP/PN blends exhibit lower storage modulus than the neat PP over the entire temperature range of the study (−40 to 50 °C). The storage moduli of PP and PP/PN blends show a rapid decrease in the temperature region associated to the glass transition temperature. At −40 °C the storage modulus for PP is 2.93 GPa, which decreases as the temperature increases, and it drops down to 1.09 GPa at 40 °C. The reason is that below glass temperature, thermal energy in the glassy region is insufficient to overcome the potential barriers for translational and rotational motions of the polymer molecular segments including changes of bond lengths and bond angles, whereas above glass transition temperature thermal energy becomes comparable to the potential energy barriers to the segmental motions.

Tan δ is another important dynamic mechanical parameter which is a measurement of damping, the relation between the elastic energy stored and the energy dissipated per cycle of vibration [22]. T_gs, obtained as the maximum of the tan δ peaks, are plotted in Fig. 2. As can be seen, T_g decreases with the increasing PN content. Based on the above results, it can be concluded that polyoxyethylene nonylphenol plays a role as plasticizer for PP which facilitates thermal motion of PP molecules leading to the decrease of T_g.

3.2. Nonisothermal crystallization behaviour by DSC

From normalized DSC curves of samples crystallized from melt at a given cooling rate, some useful parameters can be obtained to describe the nonisothermal crystallization behaviour of polymers defined below and illustrated in Fig. 3(a) [23–25]:

1. T_p, the peak temperature of crystallization. The temperature at which the value of the heat flow is maximum.
2. T_c, the temperature at the intercept of the tangents at the baseline and the high temperature side of the exotherm.
3. ΔW, the width at half-height of the exotherm peak.
4. A, the area of the normalized exotherm peak.

T_p is a function of cooling rate and is a measure of supercooling. Generally T_p shifts to low temperature with increase of cooling rate implying an increase in supercooling. The value of T_c–T_p reflects the overall crystallization rate. The smaller T_c–T_p is the greater the crystallization rate is. ΔW, determined after normalization of the exotherm peak, is a measure of the crystal size distribution; the smaller the ΔW, the narrower the size distribution of the crystallites. The area A is a quantity proportional to the heat of crystallization of the given sample. As all the measurements were done under identical settings of the instrument, the variation of A can be

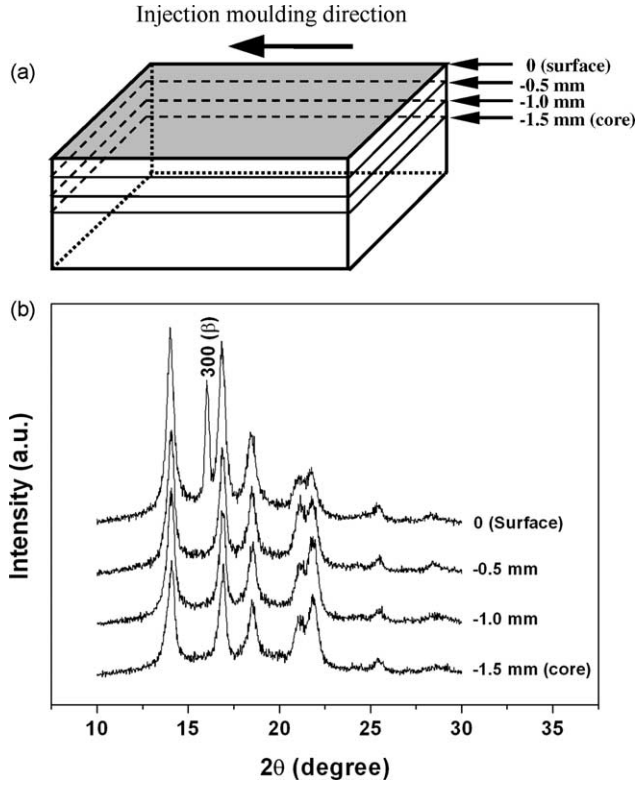

Fig. 5. The schematic of subsurface locations (a) and WAXD curves of the outside surface and subsurfaces parallel to the injection moulding direction of the tensile bar for PP/PN blend (0.75 wt%) (b).

taken to represent the variations of crystallinity in these samples.

The normalized DSC cooling thermograms of PP and PP/PN blends are shown in Fig. 3(b). Table 2 gives a summary of the nonisothermal crystallization parameters according to the normalized DSC thermograms. It can be seen that the T_p shifts to low temperature with the incorporation of PN. Generally, adding nucleation agent or inorganic fillers will reduce supercooling and result in an increase of T_p because of their heterogeneous nucleation [26–28]. The decrease of T_p for PP/PN blends means that PN not only has no acceleration nucleation effects on PP, but also depresses the formation of crystal nucleation which might be due to the dilution effect of PN. Similar nonisothermal crystallization behaviour was observed in high density polyethylene (HDPE)/ethylene-octene rubbers blends [29]. It was reported that neither the rubbers incorporated into HDPE nor their additives (stabilizers, etc.) acted as nucleation agents for HDPE. The $T_c - T_p$ values present in Table 2 show a decrease with increasing PN content indicating the crystallization rate of PP increases. The parameters of the area of the exotherm peak (A) and the width at half-height of the exotherm peak (ΔW) are also listed in Table 2. ΔW shows an increase tendency which means the crystallite size distribution of PP is narrower than that of PP/PN blends. The area of the exotherm peak (A) of the PP/PN blends are greater than that of the neat PP indicating the PP/PN blends have a higher degree of crystallinity than that of neat PP which is reasonable becasue PN acts as plasticizer facilitating molecular motion of PP as revealed by DMA.

3.3. Crystallization and orientation of injection moulded PP/PN blends by WAXD

The WAXD curves of neat PP as well as the PP/PN blends are given in Fig. 4. The neat PP shows three strong diffraction peaks at $2\theta = 13.98$, 16.80 and 18.46°, while a new sharp diffraction peak at 16.08° is observed for all the PP/PN blends. The peaks at $2\theta = 13.98$, 16.80 and 18.46° correspond respectively to the (110), (040) and (130) diffraction planes of the α-form PP crystals with a monoclinic configuration [1]. The sharp peak at 16.08° is the characteristic (300) diffraction plane of the β-form PP crystals. As we have known that quenching is favorable for the formation of β-form crystals

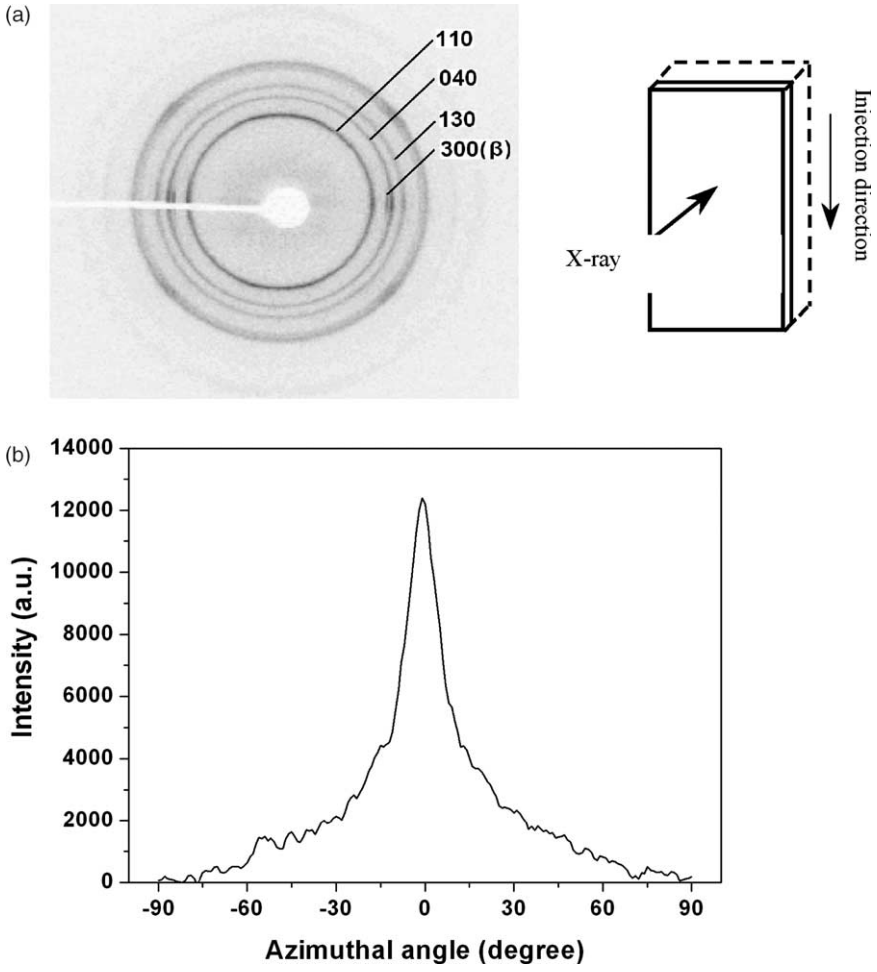

Fig. 6. WAXD pattern taken from a thin surface layer of a tensile bar parallel to the injection-moulding direction and the flat surface (a), and the azimuthal profile of (300) diffraction of β-form crystals (background contribution has been subtracted) (b).

which implies β-form crystals of PP undergo a fast folding and packing process during quenching. The incorporation of PN promotes the PP molecular motion leading to the β-form crystals only took place in PP/PN blends.

Each WAXD peak was fitted with the Gaussian distribution and its half width and area was calculated. The relative amount of the β-form PP crystals (K value) is determined by the ratio between the area of (300) diffraction peak and the sum of the area of the (110), (040) and (130) diffraction peaks as well as (300) peak. Mathematically, the K value is given by [1]

$$K = \frac{I_{300(\beta)}}{I_{110(\alpha)} + I_{040(\alpha)} + I_{130(\alpha)} + I_{300(\beta)}} \quad (1)$$

Sharper peaks, corresponding to lower values of half width, reflect a larger crystallite size. The crystallite sizes (L_{hkl}) in the direction perpendicular to the set of lattice planes having Miller Indices, hkl, were obtained by the well-known Scherrer equation [30]:

$$L_{hkl} = \frac{k\lambda}{\beta_{hkl} \times \cos\theta_{hkl}} \quad (2)$$

where k is the Scherrer constant, taken as $k \sim 0.89$; λ is the wavelength of X-ray; $2\theta_{hkl}$ is diffraction angle; β_{hkl} is the broadening due to crystallite size effects (no lattice strain is included here), and is related to the measured half width of various diffraction peaks B; and instrumental broadening parameter, b; for Gaussian line shapes using:

$$\beta^2 = B^2 - b^2 \quad (3)$$

The structural parameters determined from the WAXD curves were summarized in Table 3.

To examine the crystallization behavior in the thickness direction of injection moulded bars, subsurface layers parallel to the injection moulding direction were obtained by removing surface layers as illustrated in Fig. 5(a). The WAXD curves at different depth of PP/PN blend (0.75 wt%) are present in Fig. 5(b). As can be seen, characteristic (300) diffraction peak of β-form PP crystals takes place on the specimen surface, however, only α-form diffractions appear below surface layer. By surveying literature data on PP crystallization, Labor et al. [7] gave a schematic time–temperature-crystallization diagram for PP. It showed that there is a competition between α-form and β-form crystals during crystallization from melt, and even very fast quenching from melt can hardly avoid formation of α-form crystals, thus PP simultaneously crystallizes into α and β-forms, and their relative amounts is essentially determined by the crystallization temperature or the cooling rate. In this study, it is obvious that the surface layer cooled much faster than the subsurface layers (core) during injection moulding leading to the β-form crystal only appeared on the surface. Under surface layer, formation of β-form crystals was depressed and only α-form crystal took place.

In general, polymer molecules will orient to the injection flow direction during injection moulding, and WAXD has been proved to be a powerful technique to determine orientation. Fig. 6(a) shows the WAXD pattern of a surface layer with thickness of 0.3 mm obtained from a PP/PN (0.75 wt%) tensile bar parallel to the injection flow direction and the flat surface. The Debye rings of α-form crystals are clearly displayed. On the contrary, the β-form crystals show a pair of short Debye arcs indicating a strong orientation of β-form crystals. The reason is that β-form crystals only exist in the surface layer but α-form crystals exist in both the surface layer and the subsurface layer. Indeed, a weak orientation of α-form crystals was observed in Fig. 6(a) due to the orientation of α-form crystals in surface layer. Below the surface layer, the molecular orientation decreased leading to the Debye rings of α-form crystals. It also proved that the degree of orientation of PP crystals in the surface layer is greater than that in the core for injection moulded bars.

The azimuthal profile of (300) diffraction of β-form crystals is shown in Fig. 6(b). The orientation degree of β-form crystals can be determined by the Hermans orientation function as follows [30]:

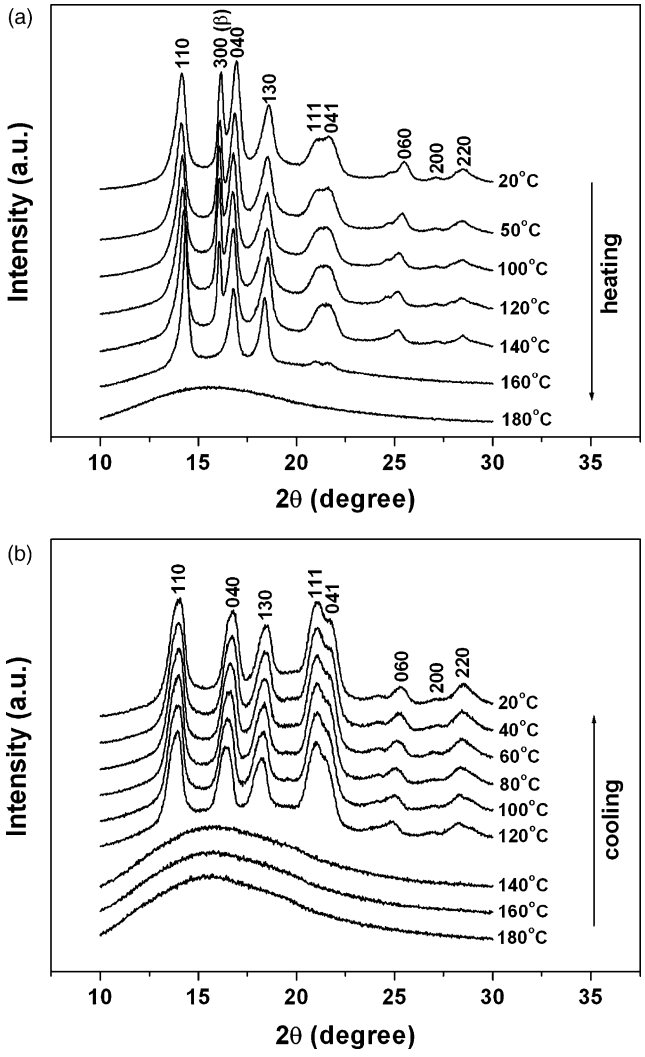

Fig. 7. High temperature WAXD curves of PP/PN blend (0.75 wt%) during heating (a) and cooling (b).

$$f = \frac{3\langle\cos^2\phi\rangle - 1}{2} \tag{4}$$

where $\langle\cos^2\phi\rangle$ was defined as

$$\langle\cos^2\phi\rangle = \frac{\int_0^{\pi/2} I(\phi)\cos^2\phi \sin\phi \mathrm{d}\phi}{\int_0^{\pi/2} I(\phi)\sin\phi \mathrm{d}\phi} \tag{5}$$

and $I(\phi)$ is the intensity along with azimuthal angle (ϕ) of the (300) diffraction. As well known, Hermans orientation function (f) takes value 1.0 when crystals are completely oriented parallel to the flow direction, 0 for the case of random orientation and −0.5 for the case of complete orientation perpendicular to the flow direction. Finally, a value of 0.43 was obtained for Hermans orientation function (f) in this study indicating the β-form crystals orientated significantly on the surface parallel to the injection moulding direction in tensile bars.

3.4. Crystallization of PP/PN blend during heating and cooling by WAXD and POM

High temperature WAXD and POM were used to evaluate the crystallization of PP/PN blends and the thermal stability of β-form crystals at high temperature. The WAXD curves of PP/PN blend (0.75 wt%) during heating are shown in Fig. 7(a). At room temperature, the diffractions of both α-form and β-form crystals are observed indicating α-form and β-form crystals coexisted. With the temperature increasing, the (300) diffraction of β-form crystals at $2\theta \sim 16.1°$ disappears above 140 °C meaning the disappearance of β-form crystals which indicates the β-form PP crystals are metastable that agrees well with the report by Lotz [31]. Fig. 7(b) shows the WAXD of PP/PN blend during cooling. As can be seen, diffractions of β-form crystals disappear indicating β-form crystals do not form during cooling which should be due to the relative slow cooling rate (5 °C/min).

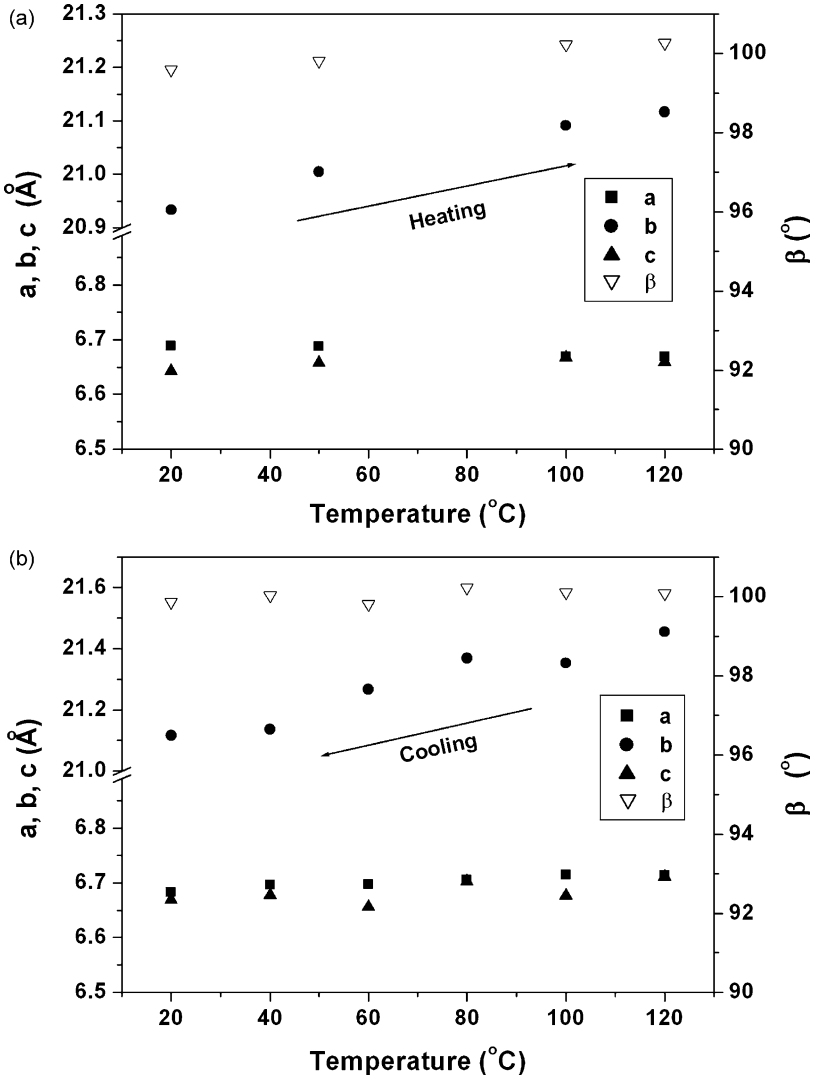

Fig. 8. The variations of the lattice parameters with temperature for PP/PN blend (0.75 wt%); heating run (a) and cooling run (b).

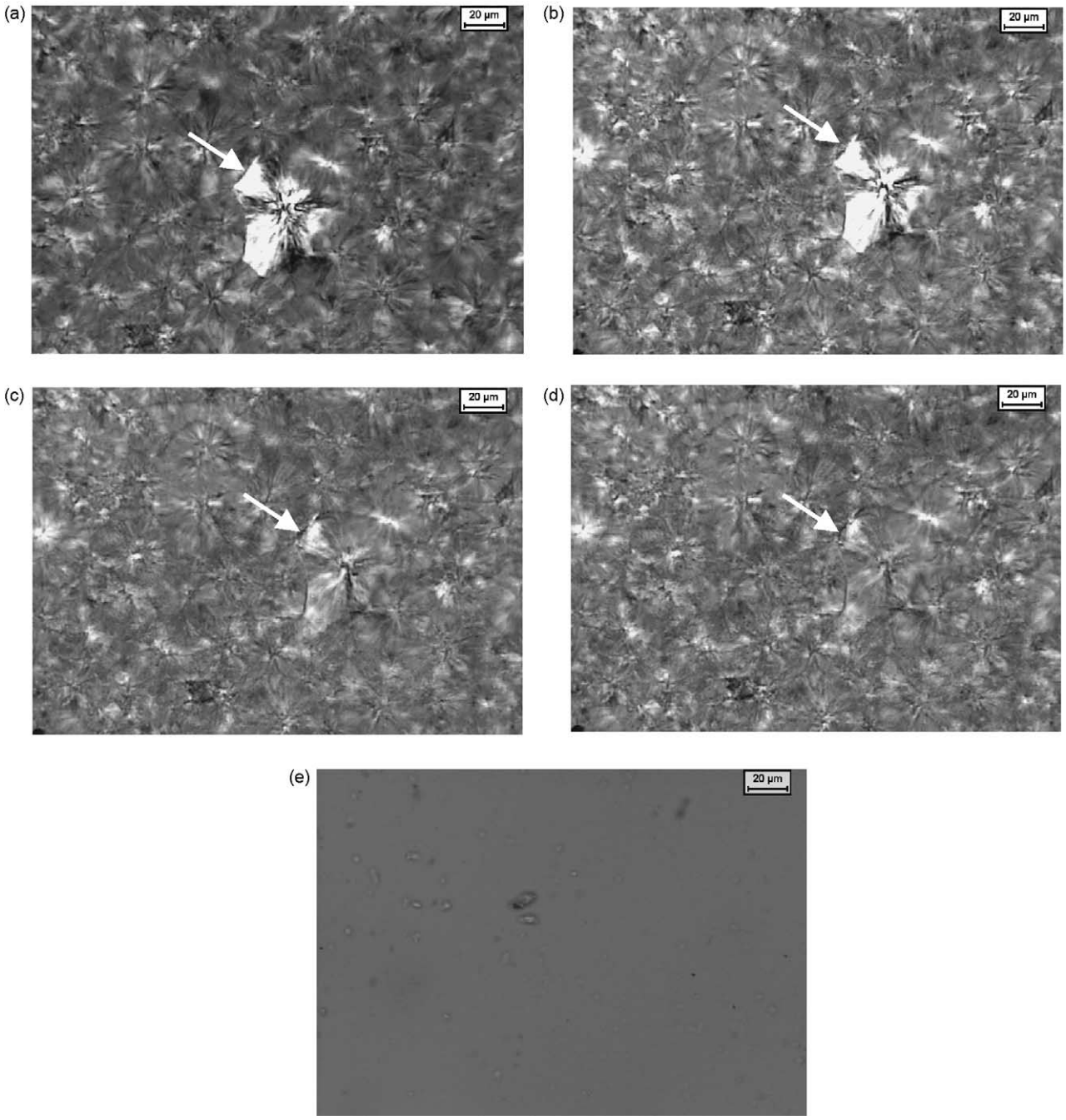

Fig. 9. POM micrographs of PP/PN blend (0.75 wt%) at RT (a), 140 °C (b), 143 °C (c), 145 °C (d) and 180 °C (e).

It is worthy of note that some diffractions shifts apparently during heating and cooling as shown in Fig. 7, i.e. (040) and (130) diffractions of α-form crystals shifts to low angle during heating and to high angle during cooling. Fig. 8 (a) and (b) present the variation in the lattice parameters of α-form crystals during heating and cooling processes respectively. The lengths of *a* and *c* axes and angle β vary slightly with increasing temperature, while the length of *b* axis increases considerably larger than those in the other axes as shown in Fig. 8(a) indicating that the *b* axis is more sensitive to temperature change than the other axes. In the cooling run as shown in Fig. 8(b), the *b* axis length decreases gradually with the decreasing temperature while the lengths of *a* and *c* axes and angle β vary slightly. It is well known a planar zigzag conformation is most stable in polyethylene (PE) crystals. The formation of the α-form crystals of PP requires interdigitation of methyl groups of rows of right handed helices onto left handed ones in the plane corresponding to the *c*–*a* axis [32,33]. The fact that, *b* axis of α-form crystals has a large variation with increasing or decreasing temperature, is a consequence of the 3_1 helical conformation of the molecular chain.

The β-form spherulite shows different morphology with α-form spherulite and can be readily distinguished from each other under polarized optical microscopy [1,31].

Fig. 9 shows a series of POM micrographs of PP/PN blend (0.75 wt%) during heating at 10 °C/min from room temperature to 200 °C. The morphology of β-form spherulites at room temperature is present in Fig. 9(a), and as can be seen β-form spherulite is stable up to 140 °C as shown in Fig. 9(b). However, the birefringence of β-form spherulites becomes blurry at 143 °C [Fig. 9(c)] while α-form spherulites show little change. At 145 °C, the birefringence of β-form spherulites disappeared and exhibited the same morphology with that of α-form spherulites [Fig. 9(d)]. It is worth noting that the shape of the β-form spherulites is still maintained at 145 °C as indicated by the arrows in Fig. 9(a)–(d) though the birefringence of β-form spherulites has disappeared. It means that a β→α growth transition takes place at 143 °C which agrees well with the WAXD results given in Fig. 7(a). Finally, all the PP spherulites melt and none birefringence of spherulites can be observed above the PP melt point [Fig. 9(e)]. Varga [1] and Lotz [31] et al. have given a rational explanation in terms of β→α growth transition in terms of crystallography. It was revealed that the α-form recrystallization phenomena taking place during β-form melting depends on growth kinetics and thermal history memory effects.

4. Conclusions

Polypropylene (PP) was blended with polyoxyethylene nonylphenol (PN) in a twin-screw extruder and then injection moulded. Polyoxyethylene nonylphenol played a role as plasticizer for PP leading to the decrease of PP glass transition temperature. Nonisothermal crystallization parameters showed that polyoxyethylene nonylphenol depressed the formation of crystal nucleation leading to the decrease of peak temperature of crystallization. The results of WAXD and POM during heating and cooling revealed that the addition of polyoxyethylene nonylphenol is helpful to form β-form crystals at rapid cooling condition which is also important as well as the addition of PN to PP. The β-form crystals orientated on the surface of injection moulded tensile bars, and its Hermans orientation function was determined to be 0.43. The disappearance of WAXD and birefringence of β-form crystals indicated that β→α growth transition took place at 143 °C as revealed by high temperature WAXD and POM. The lattice parameters of α-form crystals were determined during heating and cooling. The *b* dimension of α-form crystals underwent a large thermal expansion with temperature while the changes of the *a* and *b* axes, and angle β were small.

Acknowledgements

Q.-X. Zhang is grateful to Professor Y.-W. Mai and Dr Z.-Z. Yu of the University of Sydney for their supports.

References

[1] Karger-Kocsis J. Polypropylene structure, blends and composites. London: Chapman & Hall; 1995.
[2] Auriemma F, de Ballesteros OR, Rosa CD, Corradini P. Macromolecules 2000;33:8764–74.
[3] Tjong SC, Shen JS, Li RKY. Polymer 1996;37:2309–16.
[4] Turner-Jones A, Aizlewood JM, Beckett DR. Macromoleculare Chemie 1964;75:134–54.
[5] Natta G, Corradini P. Nuovo Cimento Suppl 1960;15:40–51.
[6] Padden FJ, Keith HD. J Appl Phys 1959;30:1479–84.
[7] Labour T, Gauthier C, Séguéla R, Vigier G, Bomal Y, Organge G. Polymer 2001;42:7127–35.
[8] Labour T, Vigier G, Séguéla R, Gauthier C, Organge G, Bomal Y. J Polym Sci, Part B: Polym Phys 2002;(40):31–42.
[9] Tjong SC, Xu SA. Polym Int 1997;44:95–103.
[10] Li JX, Cheung WL, Jia D. Polymer 1999;40:1219–22.
[11] Keith HD, Padden FJ, Walter NM, Wyckoff HW. J Appl Phys 1959;30:1485–8.
[12] Turner-Jones A, Cobbold AJ. J Polym Sci, Part B: Polym Lett 1968;6:539–46.
[13] Meille SV, Brückner S, Porzio W. Macromolecules 1990;23:4114–21.
[14] Angelloz C, Fulchiron R, Douillard A, Chabert B, Fillit R, Vautrin A, et al. Macromolecules 2000;33:4138–45.
[15] Morrow DR, Newman BA. J Appl Phys 1968;39:4944–50.
[16] Chern CS, Lin SY, Chen LJ, Wu SC. Polymer 1997;38:1977–84.
[17] Cannon LA, Pethrick RA. Polymer 2002;43:1223–33.
[18] Cannon LA, Pethrick RA. Polymer 2002;43:1249–58.
[19] Zhang D, Jiang X, Yang C. J Appl Polym Sci 2003;89:3587–93.
[20] McDermott MK, Schroeder LW, Balsis SL, Paradiso NA, Byrne ML, Briber RM. J Appl Polym Sci 2004;91:1086–96.
[21] Zhang QX, Yu ZZ, Xie XL, Mai YW. Polymer 2004;45:5985–94.
[22] Goyanes SN, König PG, Marconi JD. J Appl Polym Sci 2003;88:883–92.
[23] Gupta AK, Gupta VB, Peters RH, Harland WG, Berry JP. J Appl Polym Sci 1982;27:4669–86.
[24] Gupta AK, Purwar SN. J Appl Polym Sci 1984;29:1595–609.
[25] Jiang X, Zhang Y, Zhang Y. J Polym Sci, Part B: Polym Phys 2004;42:1181–91.
[26] Chan CM, Wu JS, Li JX, Cheung YK. Polymer 2002;43:2981–92.
[27] Liu X, Wu Q, Berglund LA. Polymer 2002;43:4967–72.
[28] Zhang QX, Yu ZZ, Yang MS, Ma J, Mai YW. J Polym Sci, Part B: Polym Phys 2003;41:2861–9.
[29] Bartczak Z, Argon AS, Cohen RE, Weinberg M. Polymer 1999;40:2331–46.
[30] Yin JH, Mo ZS. Modern polymer physics. Beijing: Science Press; 2001.
[31] Lotz B. Polymer 1998;39:4561–7.
[32] Lotz B, Wittmann JC. J Polym Sci, Part B: Polym Phys 1986;24:1541–58.
[33] Isasi JR, Alamo RG, Mandelkern L. J Polym Sci, Part B: Polym Phys 1997;35:2945–9.